Asian Journal of Chemistry; Vol. 35, No. 3 (2023), 639-648

ASIAN JOURNAL OF CHEMISTRY

https://doi.org/10.14233/ajchem.2023.27565

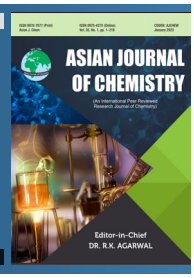

Virtual and *in vitro*, *in vivo* Screening of Transition Metal Complexes of *N*,*N*-Chelating Ligand: Experimental and Theoretical Investigations

NAZEER MOHAMED NASAR[1], MICHAEL SAMUEL[2], PORKODI JAYARAMAN[3], FREEDA SELVA SHEELA[1] and NATARAJAN RAMAN[1,*]

[1]Research Department of Chemistry, V.H.N.S.N. College (Autonomous) (Affiliated to Madurai Kamaraj University, Madurai), Virudhunagar-626001, India
[2]Department of Chemistry, P.S.R. Engineering College (Autonomous), Sivakasi-626140, India
[3]Post Graduate and Research Department of Chemistry, The Standard Fireworks Rajaratnam College for Women (Autonomous), Sivakasi-626123, India

*Corresponding author: Fax: +91 4562 281338; Tel: +91 92451 65958; E-mail: ramchem1964@gmail.com

Received: 11 January 2023; *Accepted*: 28 January 2023; *Published online*: 27 February 2023; AJC-21156

Several transition metal complexes [ML(phth)], where M = Cu(II), Zn(II), Co(II) and Ni(II), X = phthalic acid and L = Schiff base generated from benzene-1,2,diamine and 4-chlorobenzaldehyde, were synthesized and characterized by IR, UV-Vis, ^{1}H NMR, ^{13}C NMR and mass spectra. According to the physico-chemical studies, all the synthesized metal(II) complexes have a square planar geometry. The DNA nuclease activity of the synthesized metal complexes was investigated using UV absorption assay and viscosity, validating the intercalative mechanism of binding. Antimicrobial activity of the ligand and its metal(II) complexes on various microorganisms was also investigated. The optimal form and biological accessibility of the metal complexes were examined by the Gaussian 09W algorithm. These compounds were screened for drug-like activity and pharmacokinetic studies using the free SWISS ADME online software. The positive outcomes of molecular docking studies on the COVID-19 virus and cancer DNA are interesting.

Keywords: Phthalic acid, Schiff base, 4-Chlorobenzaldehyde, Benzene-1,2-diamine, CT-DNA, DFT, Molecular docking.

INTRODUCTION

Schiff base metal complexes have played a key role in the advancement of the coordination chemistry [1]. Aromatic/aliphatic aldehyde and amines when condensed, they form Schiff bases. It is an essential beauty of natural ligands which are intensely being studied. Despite the fact that this topic has received much study, transition metal Schiff base complexes continue to be the top pastime in inorganic chemistry [2]. The chelating ability and organic metal complexes have a lot of attention [3]. Over the years, metals have played a crucial role in biological structures. Adding metal ions directly to a biological systems can be achieved for diagnostic or healing purposes, despite the fact that both purposes sometimes overlap [4].

The coordination of Schiff bases with transition metals is currently being extensively examined in the fields of pharmaceuticals and diagnostics [5]. The interest in Schiff base metal complexes has grown as bioinorganic chemistry which has advanced because it has been discovered that many of these complexes can also serve as models for physiologically vital organisms [6].

In this work, the synthesis, characterization and antibacterial activity of a few transition metal(II) complexes of a novel Schiff base synthesized by the condensation of benzene-1,2-diamine and 4-chlorobenzaldehyde are reported. The electronic titrations and viscosity measurements were used to investigate the nature of DNA binding with these synthesized metal(II) complexes. Additionally, the optimal geometry and quantum mechanical parameters were also computed using the basis set B3LYP approach and the Gaussian 09W programme. The online SWISS ADME programme was used to investigate absorption, distribution, metabolism and excretion (ADME) factors in order to make predictions about the efficacy of the synthesised drugs. *In vitro* bacterial and antioxidant assays were carried out for all the synthesized compounds. To anticipate the effect of the synthesized metal(II) complexes in resistance to COVID-19, the molecular docking studies were also conducted against the major protease SARS-CoV-2.

EXPERIMENTAL

All the chemicals used were of analytical grade supplied from Sigma-Aldrich, while the metal(II) salts were purchased from E. Merck. All the organic solvents were distilled from appropriate drying agents immediately prior to use

Physical measurements: Elemental analyses (C, H and N) were performed using a Perkin-Elmer 240C elemental analyzer. Attenuated total internal reflection (ATR) solid state Infrared spectra were performed on a Bruker TENOR 27 spectrometer using a KBr pellet in the range of 4000-400 cm^{-1}. The nuclear magnetic resonance was recorded on a JEOL EX270, Bruker DPX 300, DPX 400 or AV 400 spectrometer using TMS ($SiMe_4$) as an internal reference. Absorption spectra were measured JASCO V-530 UV-VIS spectrometer at room temperature. The electrochemical studies were performed with PAR 273 potentiosat. The measurements were performed at 300 K with 10^{-3} M through nitrogen bubbling in the acetonitrile solution of the metal complex containing 0.2M TEAP. The working, counter and reference electrodes used were respectively a platinum wire, platinum coil and an SCE (saturated calomel electrode). The electrospray ionization were performed on a MICROMASS Q-TOF mass spectrometer.

Synthesis of Schiff base: Benzene-1,2-diamine (0.755 g, 5 mmol) and 4-chlorobenzaldehyde (1.81 g, 10 mmol) dissolved in ethanolic solution (50 mL each) were mixed dropwise and then refluxed for 3 h at 60-80 ºC [7]. TLC was used to monitor the reaction progress using chloroform and methanol (95:5). After being separated, the solid product was washed with water, ethanol and diethyl ether before being vacuum desiccated over anhydrous $CaCl_2$. Yield: (55%), dark brownish solid, elemental anal. calcd. (found) % of $C_{20}H_{14}Cl_2N_2$ (*m.w.* 353.24): C, 67.98 (68.00); H, 3.79 (3.99); Cl, 20.07 (20.07) and N 7.73 (7.93).

Synthesis of metal(II) complexes: Schiff base ligand and the corresponding metal(II) chlorides [Cu(II), Ni(II), Co(II) and Zn(II)] were mixed in an equimolar ratio separately. The mixture was dissolved and agitated in ethanol for around 1 h. Then, the co-ligand (phthalic acid) dissolved in the ethanolic solution was added. Following a 3 h reflux in a 100 mL round bottom flask, the resultant product was filtered off, washed with cold ethanol followed by diethyl ether and finally dried in a vacuum desiccator over anhydrous $CaCl_2$ (**Scheme-I**).

[CuL(phth)]: Yield: 53%, bluish solid. Elemental anal. calcd. (found) % of $C_{28}H_{18}N_2O_4Cl_2Cu$ (*m.w.* 581): C, 57.89 (57.69); H, 3.12 (2.91); Cl, 12.21 (12.01); N, 4.82 (4.61) and Cu, 10.94 (10.71).

[ZnL(phth)]: Yield: 52%, sandal solid. Elemental anal. calcd. (found) % of $C_{28}H_{18}N_2O_4Cl_2Zn$ (*m.w.* 583): C, 57.71 (57.51); H, 3.11 (2.91); Cl, 12.97 (10.97); N, 4.81 (4.69) and Zn, 11.22 (11.20).

[CoL(phth)]: Yield: 50%, pinkish solid. Elemental anal. calcd. (found) % of $C_{28}H_{18}N_2O_4Cl_2Co$ (*m.w.* 577): C, 58.36 (58.16); H, 3.35 (3.13); Cl, 12.30 (12.28); N, 4.96 (4.76) and Co, 10.23 (10.01).

[NiL(phth)]: Yield: 54.5, greenish solid. Elemental anal. calcd. (found) % of $C_{28}H_{18}N_2O_4Cl_2Ni$ (*m.w.* 576): C, 58.98 (58.78); H, 3.35 (3.33); Cl, 12.31 (12.29); N, 4.96 (4.76) and Ni, 9.97 (10.19%).

DNA binding studies: The interactions of the synthesized metal complexes with deoxyribonucleic acid from calf thymus (CT-DNA) were studied in 5 mM Tris-HCl/50mM NaCl buffer solution at pH 7.2 [8,9]. In this experiment, while maintaining a constant volume of synthesized metal(II) complexes (3 mL), the concentration of CT-DNA was varied from 0 to 10 μm. After each addition of CT-DNA to the metal(II) complex, the solution was allowed to stand at room temperature for 5 min at 25 ºC, an absorption spectrum was recorded and used to determine the binding constant (k_b), which was calculated from the spectroscopic titration data by plotting the line between [DNA]/(ε_a-ε_f) and [DNA].

Viscosity measurements were carried out on an Ostwald's micro-viscometer, immersed in a thermostatic water bath at constant temperature (30 ± 1 ºC). In addition, stopwatch was used to measure the fluidity times at varied concentrations of the as-prepared Schiff base imine metal(II) complexes from 10 to 60 μM, keeping the DNA concentration constant at 50 μM [10]. The measured data were plotted as $(\eta/\eta°)^{1/3}$ *vs.* [complex/DNA], where η is the viscosity of DNA and η° is the viscosity of DNA in the presence of synthesized compounds.

Molecular docking studies: Molecular docking studies were carried out using the Hex 8.00 on windows 10 professional workstation. When docking was performed with default settings, it revealed a number of possible conformations and orientations for the inhibitors at the binding site [11]. The crystal 3D structure of SARS-CoV-2 M^{pro} (PDB ID: 6M71) was collected from the online Protein Data Bank (PDB) and used as receptor protein. The water removed from chain A of receptor

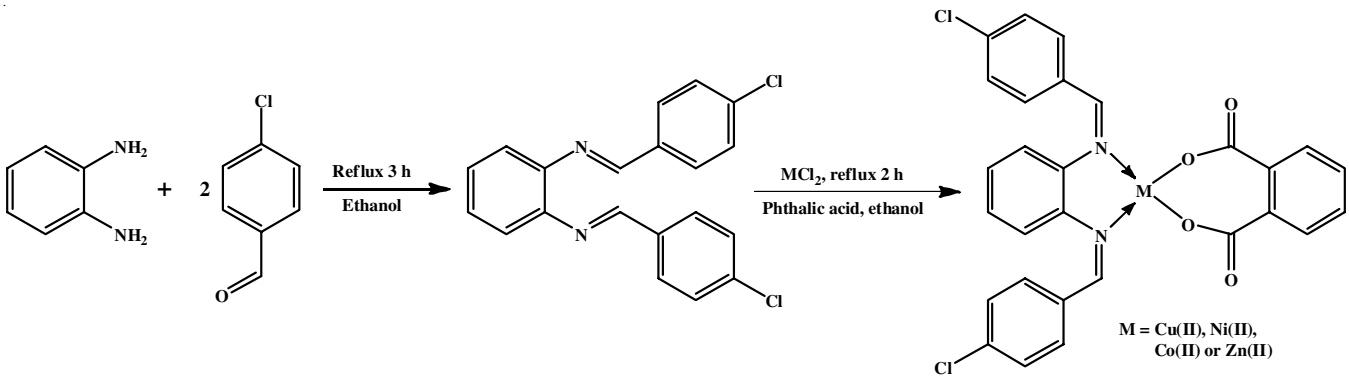

Scheme-I: Synthesis of Schiff base transition metal(II) complexes

protein by Argus lab.exe software package and saved in PDB format [11,12]. All the compounds were optimized using Avogadro version 1.2. Hex 8.00 was used headed for screen potential drugs with molecular docking by the structural protein and non-structural protein site of new corona viruses and the study was constructed to molecular docking without validation through MD simulators. Interaction with the main protease may play a key role in fighting against viruses. The results obtained from docking were visualized through Discovery studio.

DFT studies: The initial molecular geometries of synthesized compounds were optimized in the gas phase using the Gaussian 09W program package employing hybrid B3LYP/LANL2DZ+6-31+G (d,p) for the free ligand and its metal(II) complexes [13]. After determining the frequencies, the optimization process was used to get the resulting structure down to its lowest possible energy level. The Gaussian view molecular visualization program was used to visualize the input files and extract the HOMO-LUMO energies. The Koopmans theorem was used to calculate various chemical reactivity parameters such as chemical potential (μ), global hardness (η), chemical softness (S) and electrophilicity (ω) were calculated using the formula [14,15]:

$$\omega = \frac{\mu^2}{2\eta} \quad (1)$$

$$\mu = \frac{-(E_{LUMO} + E_{HOMO})}{2} \quad (2)$$

$$\eta = \frac{-(E_{LUMO} + E_{HOMO})}{2} \quad (3)$$

$$S = \frac{1}{2\eta} \quad (4)$$

Antimicrobial activity: All the synthesized compounds were tested for their antibacterial activities using broth dilution method [16] against Gram-positive bacteria *Staphylococcus aureus*, *Bacillus subtilis* and Gram-negative bacteria *Escherichia coli*, *Salmonella typhi*, *Proteus vulgaris* and antifungal activity against *Aspergillus niger*, *Candida albicans*, *Curuvulaic lunata*, *Aspergillus flavus* and *Rhizoctonia bataticola*. The MIC values of the synthe-sized compounds have been compared with the standard drugs fluconazole and ciprofloxacin [17].

***In vitro* free radical scavenger activity by DPPH assay:** DPPH (1,1-diphenyl-2-picrylhydrazyl) is a stable free radical with red colour which shows absorbance at 517 nm. If the free radicals are scavenged, DPPH will change into yellow colour. All the synthesized complexes in 10^{-4} mM and the standard vitamin C (0.1 mM) were mixed with DPPH (0.1 mM) in ethanolic solution. After 20 min incubation at room temperature, the absorbance at 517 nm was measured. The inhibitory percentage of DPPH (antioxidant activity) was calculated as follows [18,19]:

$$\text{Activity (\%)} = \frac{A_{control} - A_{sample}}{A_{control}} \times 100$$

RESULTS AND DISCUSSION

IR studies: The stretching frequency of imine (-CH=N-) of the ligand was appeared at 1595 cm^{-1}. The lowering of the double bond character of the carbon-nitrogen bond of the imine group causes the decrease in ν(-CH=N-) in all the synthesized metal(II) complexes (1573-1582 cm^{-1}) as compared to the ligand (1595 cm^{-1}). It is possible to attribute the extra bands in complexes at 1629, 1348 and 823 cm^{-1} to the vibrations of the phthalic acid moiety (Fig. 1). As a result, the two monodentate carboxylate groups that coordinate the dicarboxylic acid to the metal(II) centre make it as bidentate. The mixed phthalato complexes exhibit the phthalate group's ν(C=O) stretching vibration at 1629 cm^{-1}. Thus, the phthalato group functions as a dianionic bidentate ligand coordinated to the M(II) ion. The formation of metal-oxygen bonds in the complexes in the range of 575-550 cm^{-1} serves as an additional confirmation. The development of an M-N bond is indicated by the new band seen in the complexes in the 483-459 cm^{-1} range [20,21].

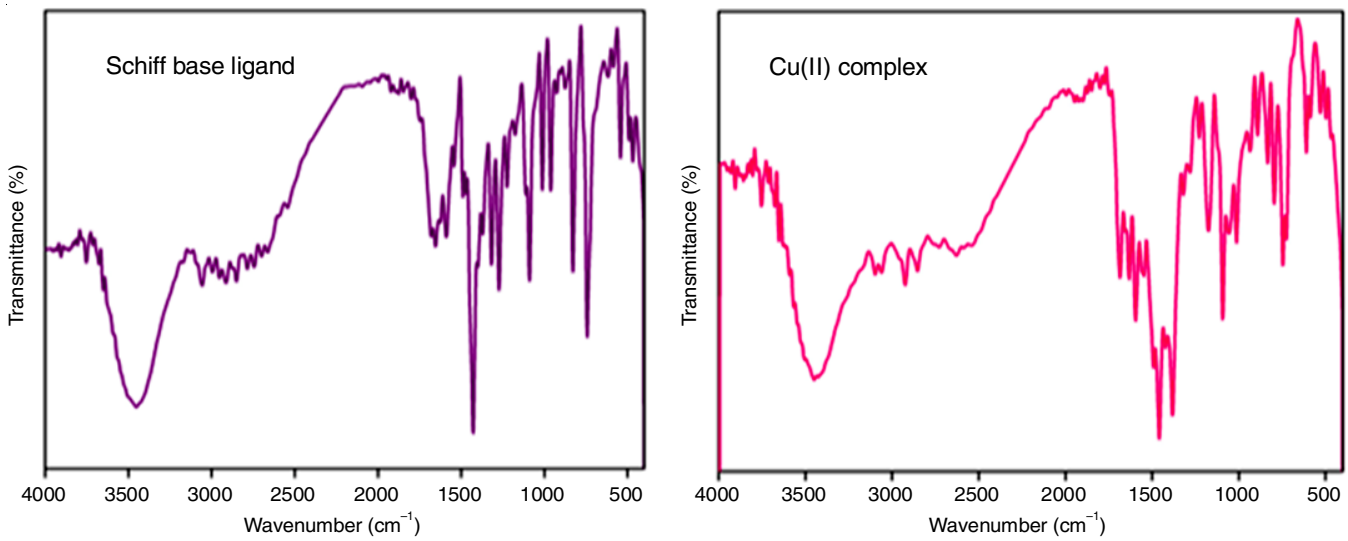

Fig. 1. FT-IR spectra of ligand and its Cu(II) complex

Electronic studies: In DMSO solution, the electronic absorbance spectra of the Schiff base ligand and its metal(II) complexes are displayed in Fig. 2. A band at 32,258 cm^{-1} is attributed to the n-π^* transition of the imine group in the Schiff base ligand. These bands are shifted to lower frequencies in the metal(II) complex spectra, indicating that the imine nitrogen atom is engaged in coordination to the metal ions. The Cu(II) complex *d-d* transition band at 17,825 cm^{-1} in the electronic spectrum strongly favours a square-planar geometry [22]. The Zn(II) complex is four coordinated and may have square-planar geometry because of its totally filled d^{10} electronic configuration, which prevents it from exhibiting a *d-d* transition. The bands at 34,482 and 31,746 cm^{-1} of the Schiff base ligand are caused by the (space) transitions of substituted aromatic moieties and imine functional groups, respectively. These peaks have been moved to a higher wavelength upon metal complexation, indicating imine nitrogen coordination. The band at 17,360 cm^{-1} in Ni(II) complex is the result of a four-coordinate square-planer geometry due to $^2A_{1g} \rightarrow {}^2A_{2g}$ transition. The broad band observed at 18,518 cm^{-1} in the electronic spectrum of the Co(II) complex is attributed to the $^4A_{2g}(F) \rightarrow {}^4T_{1g}$ transition, suggesting a square planar geometry around the Co(II) ion. Three unpaired electrons were found to have a 3.85 B.M. magnetic moment in the Co(II) complex [23].

Mass spectral studies: The molecular ion peaks and the ESI-mass spectra of the Schiff ligand and its metal complexes confirmed the suggested formulae. The [M+] peak for the Schiff base ligand is observed at *m/z* 354, which corresponds to $[C_{20}H_{14}N_2Cl_2]$ species. Also, the fragments $[C_{20}H_{15}N_2Cl]$, $[C_{20}H_{16}N_2]$, $[C_{14}H_{12}N_2]$ and $[C_8H_8N_2]$ were observed at *m/z* 319, 284, 214 and 132, respectively. The [M+] peak at *m/z* 583 was observed in the mass spectrum of complex **2** ([ZnL(phth)]). The stable species $[C_{20}H_{14}N_2Cl_2]$ exhibited the strongest peak (base beak) at *m/z* 354. The complex stoichiometry of the [ZnL(phth)] is confirmed by the *m/z* values of the ligand and its complex components. The observed peaks and their formulae, as derived from micro-analytical data, are in good accord.

^{1}H NMR studies: Using tetramethylsilane as an internal standard, the ^{1}H NMR spectra of ligand and the diamagnetic zinc(II) complex were analyzed in DMSO-d_6. The multiplet peaks in the range of 6.85 to 7.92 ppm are observed in the ^{1}H NMR study of the ligand and its Zn(II) complex, indicating the presence of an aromatic group. The imine peak for the ligand at 9.55 ppm is moved downfield to 9.85 ppm in the metal(II) complex. This downfield shift in the complex's peak relative to the ligand clearly suggests the deshielding action as the cause of the shift because it confirms the coordination of the imine nitrogen to the metal ion.

^{13}C NMR spectra: The ^{13}C NMR spectra of ligand and its Zn(II) complex. The aromatic carbon peaks can be observed in the 125-132 ppm range. Additionally, the imine group (C=N) carbons are present at 167 and 169 ppm, respectively. These peaks are shown to be pushed downfield in the Zn(II) complex, demonstrating the coordination of the (C=N) towards the metal centre.

Molar conductance: The molar conductance of each of these metal(II) complexes was evaluated at room temperature after being dissolved in DMSO. All these metal (II) complexes' molar conductance values ranged between 10.5 and 13.4 ohm^{-1} cm^2 mol^{-1}, which support their non-electrolytic nature.

In vitro analysis

DNA binding examination: By monitoring variations in the absorbance and wavelength shifts, absorption spectral titrations were used to examine the relationship between the bound chemicals and the DNA helix. Titration with electronic absorption spectroscopy is a widely used and efficient way to look at how DNA binds to a metal complex [24]. The metal complexes (**1-4**) of Cu(II), Zn(II), Ni(II) and Co(II) with DNA as well as electronic absorption spectroscopy are effective tools for investigating the binding mode and extent of ligand.

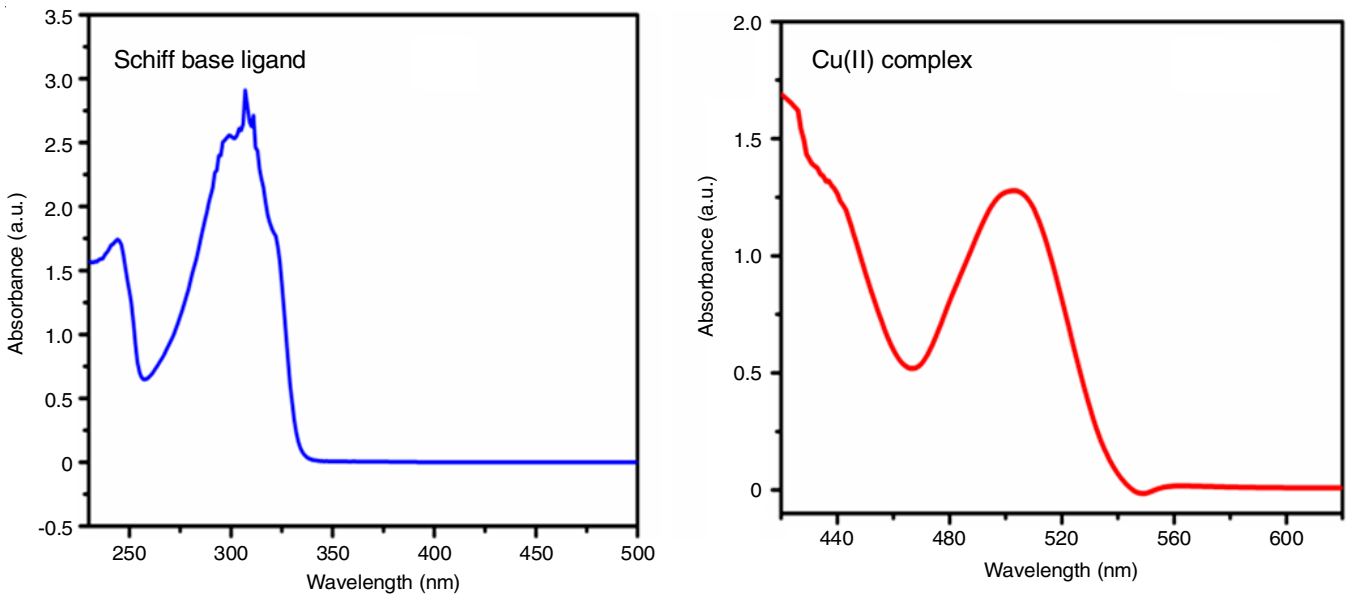

Fig. 2. Electronic absorption spectra of ligand and the Cu(II) complex

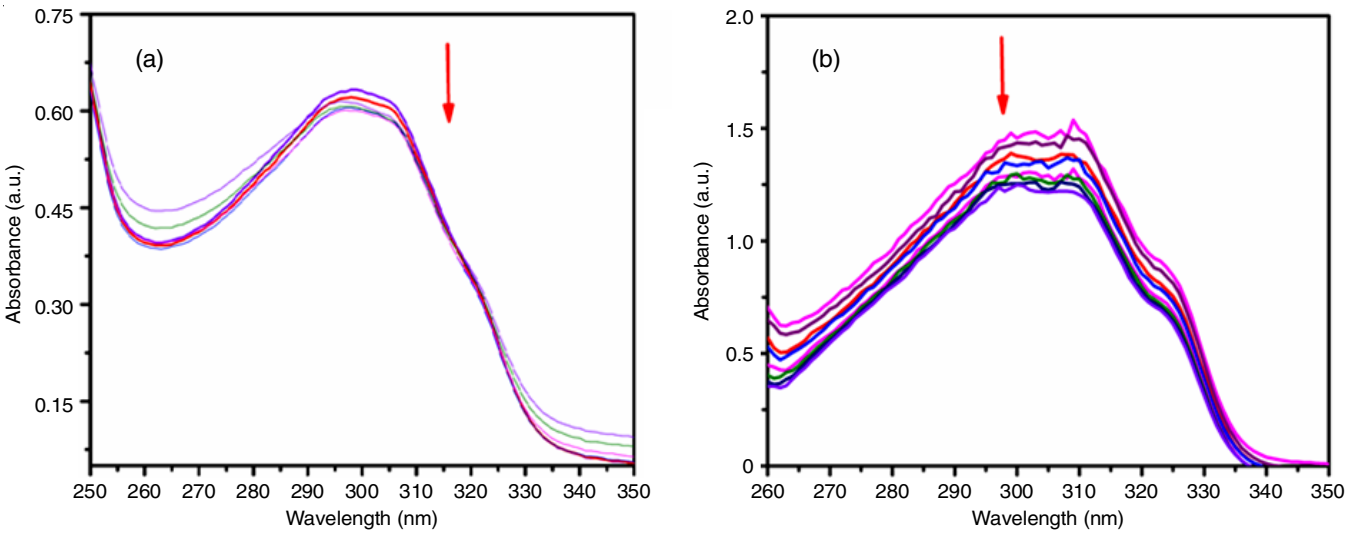

Fig. 3. (a) Absorption spectra of the 10^{-3} M DMSO solution of complex **1** in buffer (pH = 7.2) at 25 °C in presence of increasing amount of DNA, (b) Absorption spectra of the 10^{-3} M DMSO solution of complex **2** in buffer (pH = 7.2) at 25 ºC in presence of increasing amount of DNA. Arrow indicates the changes in absorbance upon increasing the DNA concentration

These spectrum characteristics point to the intercalative mode, which involves a potent stacking interaction between DNA base pairs and an aromatic chromophore. After adding DNA, the UV spectra of metal(II) complexes (**1-4**) were each recorded separately to examine the impact of the various DNA concentrations (30-180 µM). The n-π* transitions are responsible for the strong absorption in the metal complexe at wavelength ranged between 296 and 321 nm. Hypochromicity is observed alongside an increase in DNA content and a negligible red shift, both of which were measured to be in the range of 1.68 to 2.26% and 5-8 nm, respectively (Table-1) [25,26]. When hypochromism and red shift are observed, the process of binding is known as intercalation and caused by π- stacking of the aromatic phenyl rings between the DNA base pairs (Fig. 3). The intrinsic binding constants for [CuL(phth)] > [ZnL(phth)] > [NiL(phth)] > and [CoL(phth)] were found to be 5.1×10^{-4}, 4.2×10^{-4}, 3.8×10^{-4} and 3.3×10^{-5} M^{-1}, respectively. These findings imply that an intercalative mechanism of interaction between the four metal complexes and DNA.

TABLE-1
ELECTRONIC ABSORPTION SPECTRAL PROPERTIES OF Cu(II) AND Zn(II) COMPLEXES

Compound	λ_{max}		Δλ (nm)	H%[a]	$K_b \times 10^4$ $(M^{-1})^b$
	Free	Bound			
[CuL(phth)]	296	291	5	1.68	5.1
[ZnL(phth)]	309	302	7	2.26	4.2
[NiL(phth)]	321	316	5	1.55	3.8
[CoL(phth)]	317	309	8	2.25	3.3

[a]$H\% = [A_{free} - A_{bound})/A_{free}] \times 100$
[b]K_b = Intrinsic DNA binding constant determined from the UV-vis absorption spectral titration

Viscosity examination: To bolster this kind of interaction between the metal(II) complexes and DNA, viscosity measurements were added. The structural changes in DNA caused by small molecule binding have demonstrated to be the most reliable indicator of binding mode. By measuring viscosity, the DNA binding mechanism of the metal complexes **1-4** was studied. Ethidium bromide is commonly used as a strong intercalating agent in DNA binding studies, because of accommodating the ligand in between DNA base pairs that is expected to lengthen the DNA double helix. The explicit viscosities of DNA plotted against [complex]/[DNA] *vs.* $(\eta/\eta_o)^{1/3}$ is shown in Fig. 4. The least ambiguous and the most important analysis of binding in solution are considered to be hydrodynamic approaches, which are sensitive to an increase in DNA length in the absence of crystallographic structure data. A plot of $(\eta/\eta^0)^{1/3}$ *vs.* [complex] /[DNA] provides an estimation of the viscosity change. The addition of the metal(II) complexes to the DNA solution was followed by a progressive increase in the relative viscosity, which suggests that the metal(II) complexes primarily bind *via* an intercalation method. The CT-DNA relative viscosity

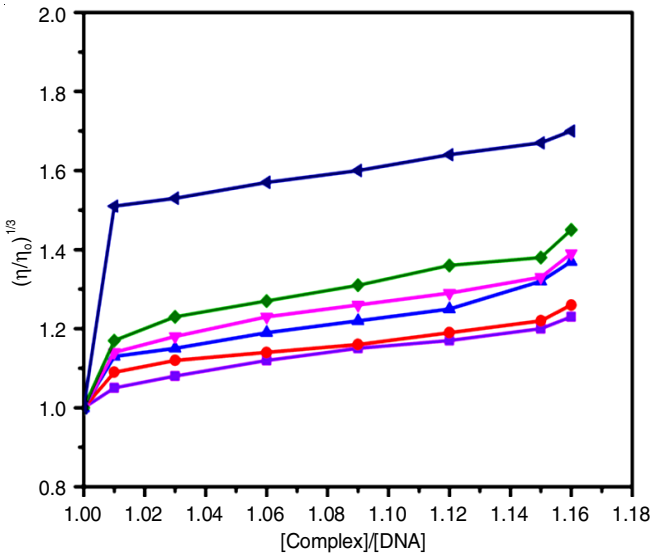

Fig. 4. Effect of increasing amount of [EB] (◀) on complexes, the 10^{-3} M DMSO solution of [CuL] (◆), [ZnL] (▼), [NiL] (▲) [CoL] (●) [L] (■) on the relative viscosity of CT DNA. Plot of relative viscosity $(\eta/\eta_o)^{1/3}$ *vs.* [complex]/[DNA]

TABLE-2
MINIMUM INHIBITORY CONCENTRATION OF THE SYNTHESIZED METAL(II) COMPLEXES AGAINST THE GROWTH OF BACTERIAL AND FUNGI (μM)

Compound	MIC values ($\times 10^4$ μM) SEM = ± 1.2									
	Bacterial activity					Fungal activity				
	S. aureus	*P. vulgaris*	*E. coli*	*B. subtilis*	*S. typhi*	*A. niger*	*A. flavus*	*C. lunata*	*R. bataticola*	*C. albicans*
Ligand	16.6	15.7	16.4	15.9	14.8	12.9	13.6	15.4	11.7	15.9
[CuL(phth)]	3.3	3.8	2.7	3.2	3.6	4.4	3.7	4.7	4.5	5.5
[ZnL(phth)]	4.1	4.4	3.7	4.4	4.9	5.3	4.8	5.9	6.6	5.3
[NiL(phth)]	4.6	5.1	4.1	4.6	5.3	6.1	5.5	6.5	7.1	7.4
[CoL(phth)]	5.3	5.5	4.6	5.1	5.6	6.5	5.9	6.9	7.5	7.9
Ciprofloxacin	1.8	1.7	2.1	1.9	2.6	–	–	–	–	–
Fluconazole	–	–	–	–	–	1.1	1.4	1.1	1.3	1.9

increases in the following order: 1 > 2 > 3 > 4 (Fig. 4). The behaviour observed in the electronic absorption spectral titration analysis are in good agreement by these results [27,28].

Antimicrobial activity: The synthesized ligand and its metal(II) complexes were examined for their *in vitro* antibacterial activites. The fungi *Aspergillus niger*, *Aspergillus flavus*, *Culvularis lunata*, *Rhizoctonia bataticola* and *Candida albicans* were tested against as well as bacteria such *Bacillus subtilis*, *Staphylococcus aureus*, *Salmonella typhi*, *Proteus vulgaris* and *Escherichia coli* [29]. Table-2 displays the minimum inhibitory concentration values. Fluconazole and ciprofloxacin were the standard drugs of choice for treating bacteria and fungus.

Comparing the MIC values of the ligand and its metal(II) complexes, the synthesized metal(II) complexes show more antibacterial activity than the ligand. The Tweedy's chelation [30] theory was used to explain the higher antibacterial activity of the complexes. In comparison to the Schiff base ligand, the metal complexes exhibit stronger antibacterial activity against bacteria and fungi.

Antioxidant activity: Through the DPPH assay, Schiff base ligand and its corresponding metal complexes were tested for antioxidant activity (free radical scavenging activity). At 517 nm, the odd electron in the DPPH exhibits a significant absorption maximum. When metal(II) complexes were added, the visible portion of DPPH exhibits significant absorbance at 517 nm and this absorbance will decrease. The stable DPPH free radical is reduced and transformed into 1,1-diphenyl-2-picrylhydrazine by obtaining an electron from an antioxidant chemical, which results in the decolorization of the DPPH solution. The antioxidant activity in copper complex is higher than those in other complexes but lower than those in ascorbic acid (Table-3). These findings revealed that copper complex has an excellent antioxidant activity [31,32].

TABLE-3
PERCENTAGE OF ANTIOXIDANT ACTIVITY OF SCHIFF BASE LIGAND AND ITS METAL COMPLEXES

Compound	Concentration (μg/mL)			
	10	20	30	40
L	45.36	53.13	57.26	61.25
[CuL(phth)]	71.24	77.28	85.35	89.13
[ZnL(phth)]	68.23	74.19	81.25	86.27
[NiL(phth)]	66.13	71.25	77.36	81.36
[CoL(phth)]	64.18	69.27	72.36	80.38
Vitamin C	80.78	86.37	89.21	93.38

ADMET properties

***In silico* studies:** Using various web tools, the ADME properties of the synthesized compounds have been evaluated before *in vivo* studies. SWISS ADME online service was used to find the molecular properties of the compounds like log P, hydrogen bond acceptors, donors, biological active score, TPSA, *etc*. Table-4 shows the pharmacokinetics properties retrieved by SWISS ADME software. These values are compared with Lipinski's rule of five and were found to possess drug like property by the lower log P value (must be less than 5), good total polar surface area value, number of rotatable bond, hydrogen acceptors and donors values. Moreover, the biological active score is higher for the synthesized compounds revealed the drug like character [33,34].

DFT studies: Theoretical quantum mechanical calculation was performed in Gaussian 09W software using B3LYP basis set. The optimized geometry, FMO and stability of the synthesized compounds were studied theoretically for all the synthesized compounds. Figs. 5 and 6 show the optimized geometry of the synthesized metal(II) complexes. The HOMO and LUMO energies of the synthesized compounds are given in Fig. 7 [35].

TABLE-4
PREDICTION OF *in silico* ADMET PROPERTIES OF THE METAL(II) COMPOUNDS

Compound	Physico-chemical properties						Bio activity score
	TPSA (Å²)	Molar refractivity	Synthetic accessibility	Number of H-acceptors	Number of H-donors	Number of rotatable bonds	
L	24.72	103.85	2.73	2	0	2	0.17
[CuL(phth)]	77.32	147.78	4.53	4	0	4	0.55
[ZnL(phth)]	77.32	147.78	4.32	4	0	2	0.55
[NiL(phth)]	77.32	147.78	4.12	4	0	2	0.55
[CoL(phth)]	77.32	147.78	4.35	4	0	2	0.55

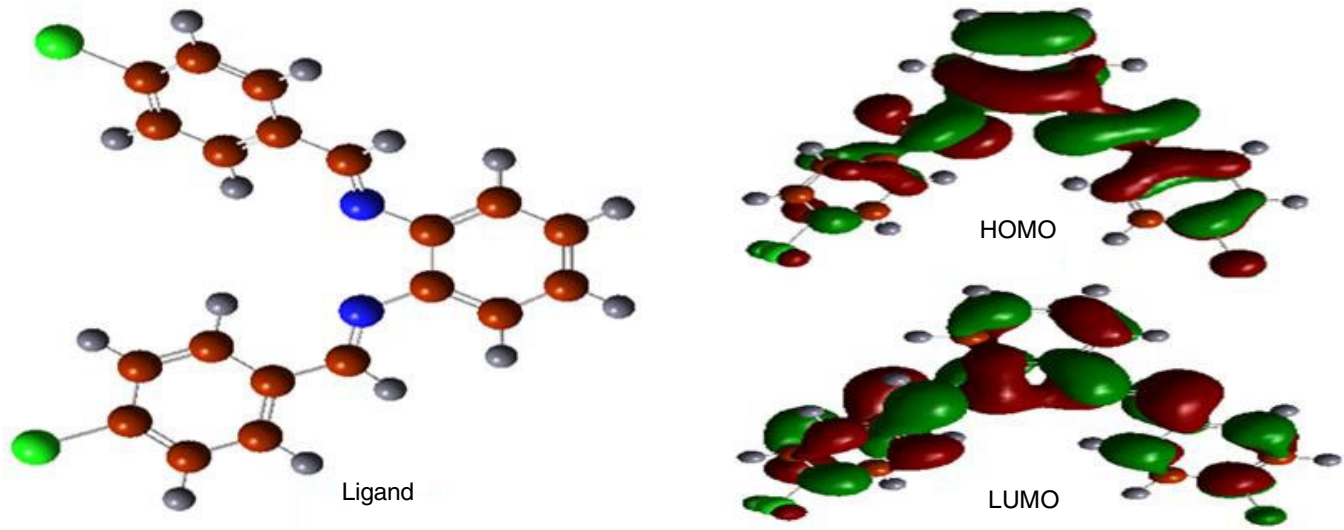

Fig. 5. HOMO-LUMO for the optimized molecular structure of Schiff base in vacuum using DFT/B3LYP/6-31G(d)basic set

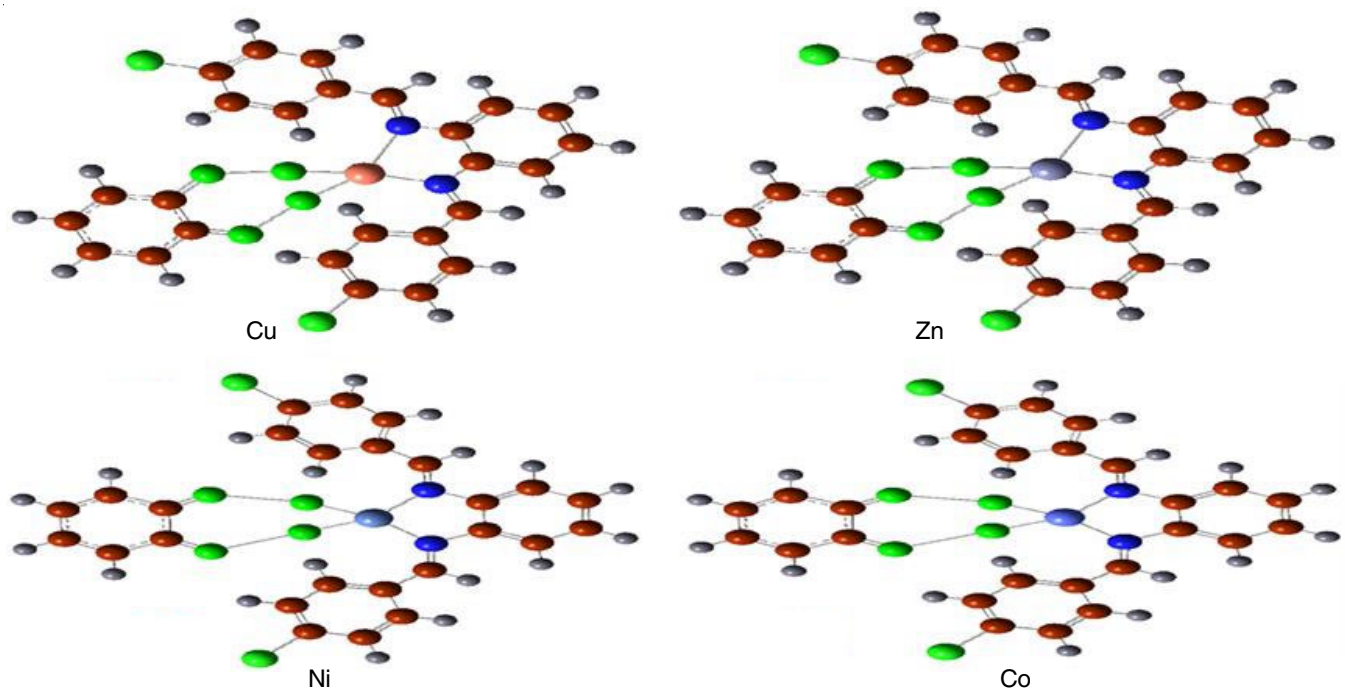

Fig. 6. Optimized molecular structure of metal(II) complexes in vacuum using DFT/B3LYP/6-31G(d) basic set

The quantum mechanical parameters were calculated and are shown in Table-5. In HOMO, the electron density is present near the hetero-atom and the aromatic moieties for all the metal complexes and the LUMO is mainly present near the coordination site of Co(II), Cu(II), Ni(II) and Zn(II) complexes. But in copper complex, the LUMO is present near the aromatic group of the co-ligand. All the synthesized compounds are stable since both the HOMO and LUMO values are negative. As the ΔE (eV) value of the metal(II) complexes is greater than that of ligands, this means that metal complexes are more stable, harder and less brittle than ligands. The ligand due to its soft nature is more elastic and active towards the coordination with metal ions [36]. The copper(II) complex has the highest dipole moment of all the synthesized compounds, suggesting it has the strongest biological interaction with living things.

Molecular docking studies: SARS-CoV-2 receptor structure was retrieved from PDB and the water present in them is removed by Discovery Studio Viswalizer 4.0 software. In present study, the molecular docking was carried out in Hex 8.0 software. All the synthesized compounds efficiently bind with the receptor by means of hydrogen bonding with the amino acids present in it. The docking scores and the amino acids bind with synthesized compounds are listed in Table-6. The major amino acids present in the active site of the receptors were ARG, ALA, TYR, LEU, LYS and THR (Figs. 8 and 9). Among all the compounds, the copper(II) complex undergoes more effective docking with receptor because of its lowest docking score value –362.00 KJ mol^{-1}. This study reveals the anti-SAR CoV-2 inhibitory action of the synthesized compounds [37,38].

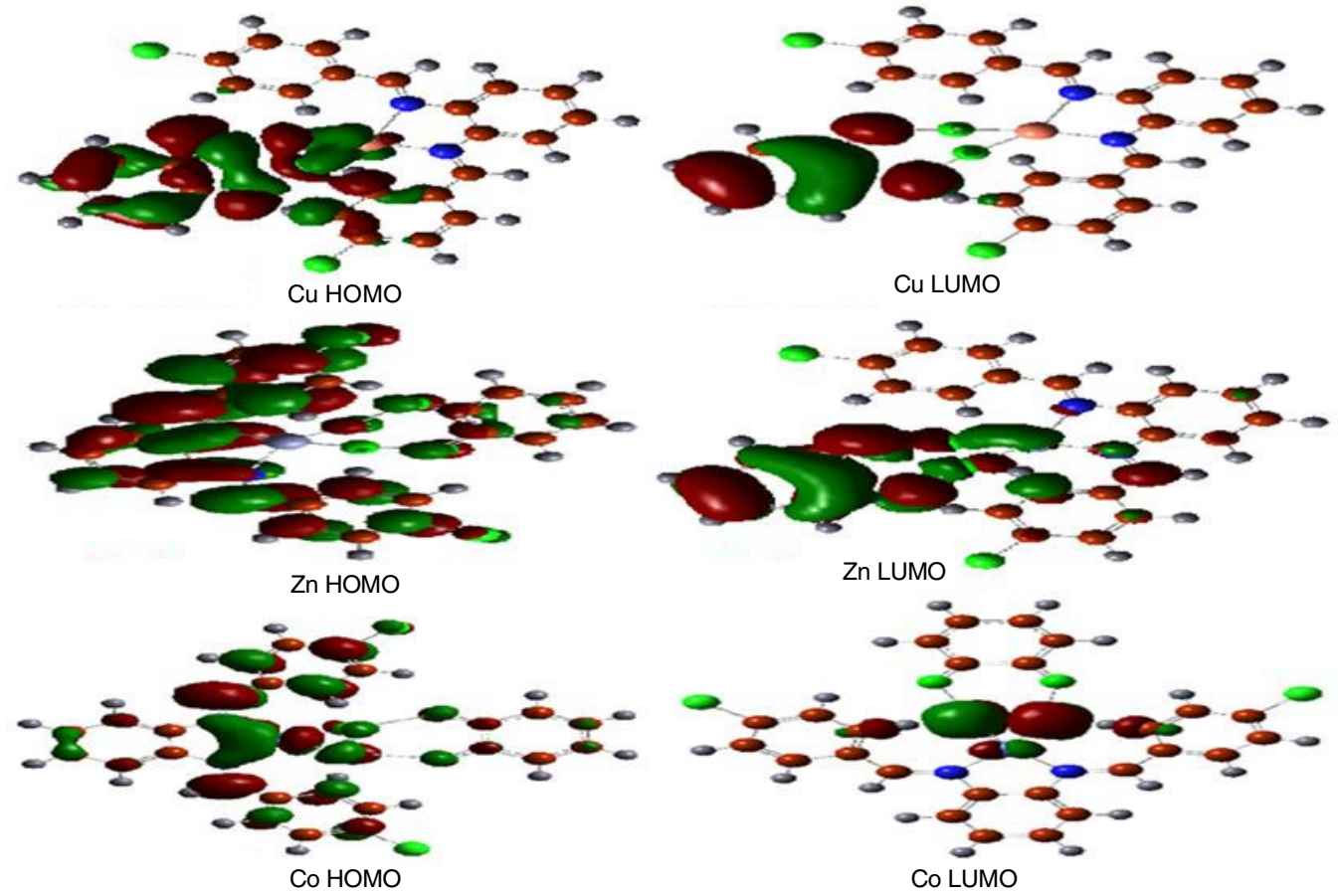

Fig. 7. Illustrative presentation of frontier molecular orbital of metal(II) complexes obtained using B3LYP/6-31G (d)basis set

TABLE-5
COMPUTATIONAL LIGAND AND TRANSITION METAL COMPLEXES IN GAUSSIAN SOFTWARE 09W

Parameter	Ligand	[CuL(phth)]	[ZnL(phth)]	[NiL(phth)]	[CoL(phth)]
ΔH_f	-1800.17	-4110.44	-3971.672	-3840.00	-3714.48
Dipole moment (Debye)	4.41	14.39	10.23	5.70	4.28
HOMO	-0.19893	-0.1877	-0.1377	-0.1783	-0.1491
LUMO	-0.0626	-0.1055	-0.1168	-0.1416	-0.1205
ΔE (eV)	0.0824	0.2932	0.2546	0.3199	0.2697
Electronegativity (χ) eV	0.02135	0.0411	0.0793	0.0183	0.0143
Global hardness (η)	0.0412	0.1466	0.1272	0.1599	0.1348
Global softness (S)	0.0206	0.0733	0.0636	0.0799	0.0674
Electrophilicity (ω)	0.0055	0.0057	0.0494	0.0010	0.0007

Conclusion

In this study, the Schiff base metal(II) complexes of copper, zinc, cobalt and nickel were synthesized and characterized using spectroscopic and analytical techniques. The Schiff base ligand was obtained from the condensation of benzene-1,2-diamine and 4-chlorobenzaldehyde. Analytical and spectral tests revealed that the ligand coordinates to the metallic ions through the nitrogen and phenolic oxygen atoms and is structured as a square planar geometry. The synthesized metal(II) complexes have undergone *in vitro* antioxidant screening for

TABLE-6
DOCKING SCORES FOR SYNTHESIZED COMPOUNDS WITH 7AEH PROTEASE OF SARS-CoV-2 TARGET AND THEIR INTERACTING AMINO ACIDS

Name of the compounds	Binding score (KJ mol^{-1})	Interacting amino acid
Ligand	-284.77	TYR46, ILE96, ARG48, TYR59, ALA50, ARG52, THA9, LEU5, ASN7
[CuL(phth)]	-362.00	LEU64, ARG52, LYS62
[ZnL(phth)]	-360.64	THR69, ALA50, ARG52, ALA50, ASN8, LEU5
[NiL(phth)]	-353.89	ARG48, TYR69, ARG67
[CoL(phth)]	-351.37	ARG52, ALA50, TYR69, ARG67

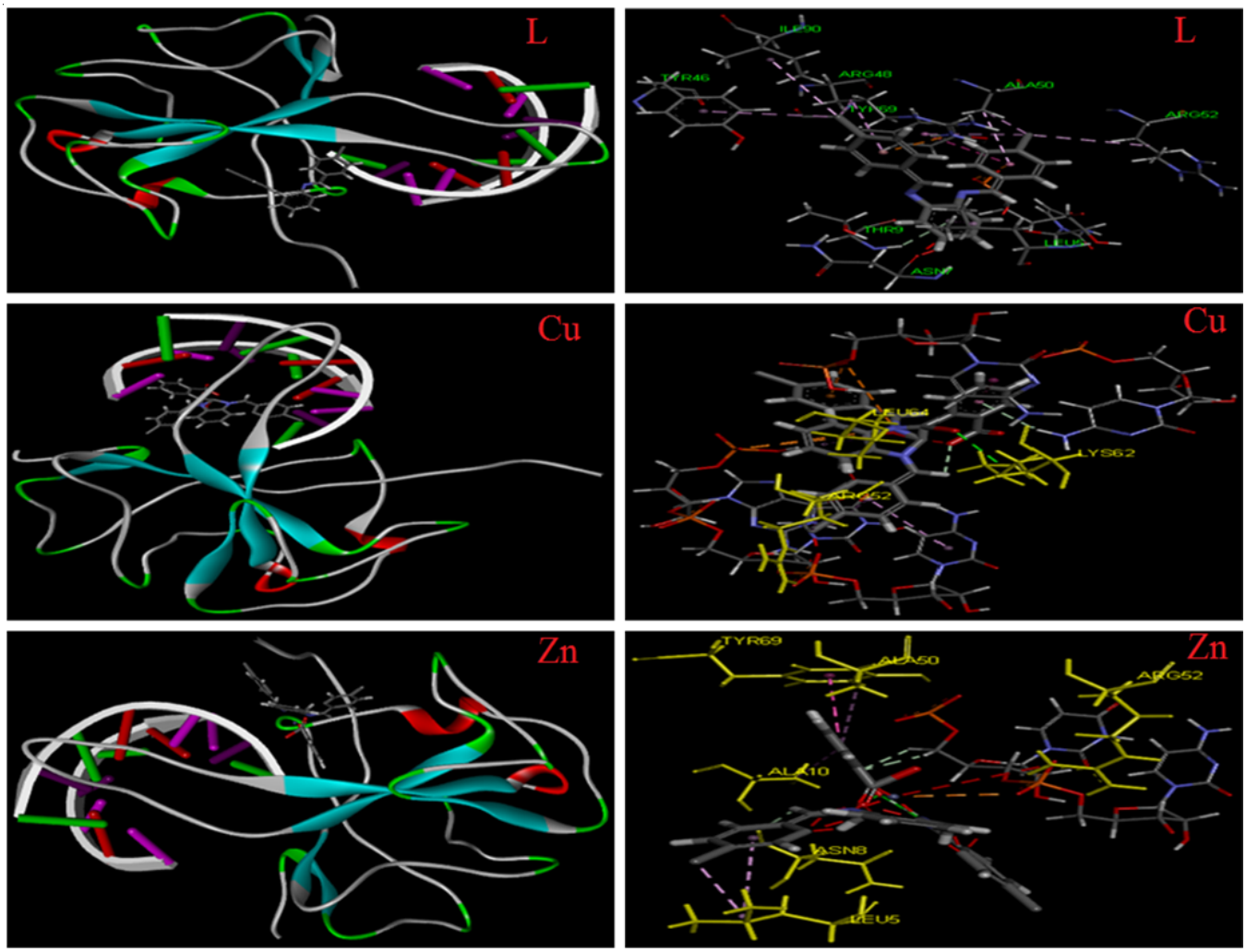

Fig. 8. Molecular docking SARS Cov receptor 7ACS of the ligand. Three dimension(3D) binding interaction of Ligand, Cu(II) and Zn(II) complexes with DNA (SARS Cov receptor 7ACS)

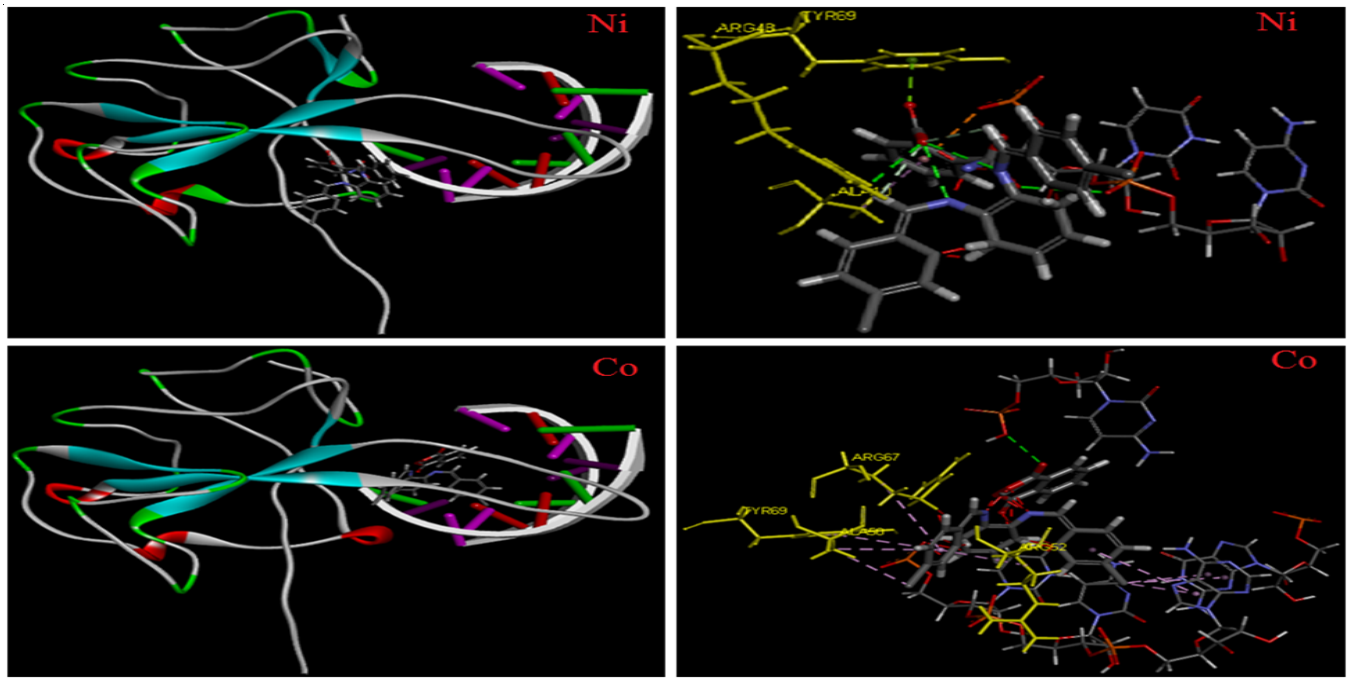

Fig. 9. Three dimension(3D) binding interaction of Ni(II) and Co(II) complexes with DNA (SARS CoV receptor 7ACS)

protection against the DPPH free radical receptor. Using theoretical DFT calculations, the Cu(II) complex exhibits a higher affinity for binding, according to *in vitro* interaction investigations of all the complexes with CT-DNA carried out using UV-Vis and viscometry methods. The aforementioned findings demonstrated that the complexes' intercalative DNA binding, which was further corroborated by a molecular docking studies. The observed *in silico* analysis also demonstrated that Cu(II) complex has significant biological action.

ACKNOWLEDGEMENTS

The authors express their sincere thanks to their respective The Principal and Head of the Department for providing the research facilities and their constant encouragement.

CONFLICT OF INTEREST

The authors declare that there is no conflict of interests regarding the publication of this article.

REFERENCES

1. N. Ahmed, M. Riaz, A. Ahmed, M. Bhagat, *Int. J. Inorg. Chem*., **2015**, 607178 (2015); https://doi.org/10.1155/2015/607178
2. N.H. Patel, H.M. Parekh and M.N. Patel, *Transition Met. Chem.*, **30**, 13 (2005); https://doi.org/10.1007/s11243-004-3226-5
3. S.H. Sumrra, M. Ibrahim, S. Ambreen, M. Imran, M. Danish and F.S. Rehmani, *Bioinorg. Chem. Appl.*, **2014**, 812924 (2014); https://doi.org/10.1155/2014/812924
4. N.A. Bitu, S. Hossain, N. Islam, A. Kader, M.S. Islam, M.M. Haque, F. Hossen, A. Asraf, R.K. Mohapatra and Kudrat-E-Zahan, *Russ. J. Gen. Chem.*, **90**, 1553 (2019); https://doi.org/10.1134/S1070363220080253
5. X.-M. Zhang, H. Guo, Z.-S. Li, F.-H. Song, W.-M. Wang, H.-Q. Dai, L.-X. Zhang and J.-G. Wang, *Eur. J. Med. Chem.*, **101**, 419 (2015); https://doi.org/10.1016/j.ejmech.2015.06.047.
6. A.M. Abu-Dief and I.M. Mohamed, *Beni-Suef Univ. J. Appl. Sci.*, **4**, 119 (2015); https://doi.org/10.1016/j.bjbas.2015.05.004
7. N. Pravin and N. Raman, *Inorg. Chem. Commun.*, **36**, 45 (2013); https://doi.org/10.1016/j.inoche.2013.08.001
8. F.T. Elmali, *J. Mol. Struct.*, **1261**, 132900 (2022); https://doi.org/10.1016/j.molstruc.2022.132900
9. E. Oguzcan, Z. Koksal, T. Taskin-Tok, A. Uzgoren-Baran and N. Akbay, *Spectrochim. Acta A Mol. Biomol. Spectrosc.*, **270**, 120787 (2022); https://doi.org/10.1016/j.saa.2021.120787
10. S.V. Aswathy, I.H. Joe and K.B. Rameshkumar, *J. Mol. Struct.*, **1263**, 133152 (2022); https://doi.org/10.1016/j.molstruc.2022.133152
11. M.N. Uddin, M.S. Amin, M.S. Rahman, S. Khandaker, W. Shumi, M.A. Rahman and S.M. Rahman, *Appl. Organomet. Chem.*, **35**, e6067 (2021); https://doi.org/10.1002/aoc.6067
12. A. Senocak, N.A. Tas, P. Taslimi, B. Tüzün, A. Aydin and A. Karadag, *J. Biochem. Mol. Toxicol.*, **36**, e22969 (2022); https://doi.org/10.1002/jbt.22969
13. H.M.A. El-Lateef, M.M. Khalaf, M.R. Shehata and A.M. Abu-Dief, *Int. J. Mol. Sci.*, **23**, 3994 (2022); https://doi.org/10.3390/ijms23073994
14. R. Nandhini, G. Venkatachalam, M. Deepan Kumar and M. Jaccob, *Polyhedron*, **158**, 183 (2019); https://doi.org/10.1016/j.poly.2018.10.058
15. A.A. Sharfalddin, A.H. Emwas, M. Jaremko and M.A. Hussien, *New J. Chem.*, **45**, 9598 (2021); https://doi.org/10.1039/D1NJ00293G
16. M. Balouiri, M. Sadiki and S.K. Ibnsouda, *J. Pharm. Anal.*, **6**, 71 (2016); https://doi.org/10.1016/j.jpha.2015.11.005
17. M. Gupta, B.K. Sarma, S. Chandra, S. Gupta and S. Singhal, *Int. J. Therap. Appl.*, **35**, 29 (2018).
18. Q.H. Tran and T.T. Doan, *New J. Chem.*, **44**, 13036 (2020); https://doi.org/10.1039/D0NJ01159B
19. M.F. Hassa, S. Hussein, Y. El Senosi, M. Kamal Mansour and A. Amin, *J. Clin. Exp. Pathol.*, **8**, 2161 (2018); https://doi.org/10.4172/2161-0681.1000346
20. G.B. Bagihalli, P.G. Avaji, S.A. Patil and P.S. Badami, *Eur. J. Med. Chem.*, **43**, 2639 (2008); https://doi.org/10.1016/j.ejmech.2008.02.013
21. F. Arjmand, F. Sayeed and M. Muddassir, *J. Photochem. Photobiol. B*, **103**, 166 (2011); https://doi.org/10.1016/j.jphotobiol.2011.03.001
22. M. Shakir, A. Abbasi, A.U. Khan and S.N. Khan, *Spectrochim. Acta A Mol. Biomol. Spectrosc.*, **78**, 29 (2011); https://doi.org/10.1016/j.saa.2010.02.034
23. N. Shahabadi, S. Kashanian and F. Darabi, *Eur. J. Med. Chem.*, **45**, 4239 (2010); https://doi.org/10.1016/j.ejmech.2010.06.020
24. N. Ganji, A. Rambabu, N. Vamsikrishna, S. Daravath and Shivaraj, *J. Mol. Struct.*, **1173**, 173 (2018); https://doi.org/10.1016/j.molstruc.2018.06.100
25. P. Jeyaraman, A. Alagarraj and R. Natarajan, *J. Biomol. Struct. Dyn.*, **38**, 488 (2020); https://doi.org/10.1080/07391102.2019.1581090
26. N. Raman, S. Sobha and M. Selvaganapathy, *Monatsh. Chem.*, **143**, 1487 (2012); https://doi.org/10.1007/s00706-012-0718-4
27. N. Raman, S. Sobha and L. Mitu, *J. Saudi Chem. Soc.*, **17**, 151 (2013); https://doi.org/10.1016/j.jscs.2011.03.003
28. N. Pravin, V. Devaraji and N. Raman, *Int. J. Biol. Macromol.*, **79**, 837 (2015); https://doi.org/10.1016/j.ijbiomac.2015.06.001
29. R. Ramesh and S. Maheswaran, *J. Inorg. Biochem.*, **96**, 457 (2003); https://doi.org/10.1016/S0162-0134(03)00237-X
30. N. Raman, R. Jeyamurugan, R. Senthilkumar, B. Rajkapoor and S.G. Franzblau, *Eur. J. Med. Chem.*, **45**, 5438 (2010); https://doi.org/10.1016/j.ejmech.2010.09.004
31. S. Daravath, A. Rambabu, N. Vamsikrishna, N. Ganji and S. Raj, *J. Coord. Chem.*, **72**, 1973 (2019); https://doi.org/10.1080/00958972.2019.1634263
32. K.S. Abou-Melha, G.A. Al-Hazmi, I. Althagafi, A. Alharbi, F. Shaaban, N.M. El-Metwaly, M.A. El-Bindary and M.A. El-Bindary, *J. Mol. Liq.*, **334**, 116498 (2021); https://doi.org/10.1016/j.molliq.2021.116498.
33. B. Mohan and M. Choudhary, *J. Mol. Struct.*, **1246**, 131246 (2021); https://doi.org/10.1016/j.molstruc.2021.131246
34. M. Samuel, R. Rajasekar, P. Jeyaraman, S. Muthusamy, V. Muniyandi and N. Raman, *Inorg. Chim. Acta*, **533**, 120783 (2022); https://doi.org/10.1016/j.ica.2021.120783
35. E. Bilen, Ü.Ö. Özmen, S. Çete, S. Alyar and A. Yasar, *Chem. Biol. Interact.*, **360**, 109956 (2022); https://doi.org/10.1016/j.cbi.2022.109956.
36. B. Marimuthu, S. Saravanaselvam, S. Michael, P. Jeyaraman and X. Arulannandham, *J. Biomol. Struct. Dyn.*, (2022); https://doi.org/10.1080/07391102.2022.2056509
37. R. Reshma, R. Selwin Joseyphus, D. Arish, R.J. Reshmi Jaya and J. Johnson, *J. Biomol. Struct. Dyn.*, **40**, 8602 (2022); https://doi.org/10.1080/07391102.2021.1914171
38. J. Porkodi and N. Raman, *Appl. Organomet. Chem.*, **32**, e4030 (2018); https://doi.org/10.1002/aoc.4030